Experimental Investigation on Advanced Composite-Stiffened Structures Under Uniaxial Compression and Bending

Giulio Romeo*
Polytechnic Institute of Turin, Turin, Italy

Several tests were conducted on graphite/epoxy hat-and blade-stiffened panels under uniaxial compression and wing-box beams under pure bending to verify the accuracy of the theoretical analysis. Theoretical analysis of the compression panels is based on both wide column and simply supported orthotropic plate theory to predict overall buckling, on orthotropic buckling equations to predict local buckling, and on a torsional instability theory for the blade-stiffened panels. Adequate correlations with experimental results were obtained for uniaxial compression when the Euler or torsional buckling modes were critical; buckling occurred at lower strain values than predicted when the local buckling mode was critical. Indeed, simple compression tests cannot represent the load conditions of wing-box compression panels properly; in particular, the bending curvature causes a distributed load perpendicular to panels that can reduce the longitudinal load at which buckling occurs.

Nomenclature

A_{ij}	= laminate extensional stiffnesses
b_i	= element widths
D_i, D_{ij}	= plate and laminate bending stiffnesses, respectively
E_{11}, E_{22}	= Young's modulus of composite material in fiber direction and normal to fiber direction, respectively
EI	= bending stiffness of beam
EI_0	= polar bending stiffness of the strut about shear center
G_{12}	= shear modulus of composite material
GJ	= beam torsional stiffness
K_R	= beam rotational stiffness
L	= panel length
M_b	= bending moment
Nx_{cr}, Nx_E	= overall and Euler buckling load per unit width of panel
p	= stiffener spacing
p_0	= distributed lateral load
P_E, P_{tors}	= Euler and torsional buckling loads of panel, respectively
P_F	= failure load of panel
W/BL^2	= mass index
t_i	= element thicknesses
ϵ_a	= allowable axial strain in each lamina
$\epsilon_E, \epsilon_{li}, \epsilon_{tors}$	= Euler, local, and torsional buckling strains, respectively
$\bar{\epsilon}_F$	= average axial failure strain
λ, μ	= buckling half-wavelength in the x and y directions, respectively
ν_{12}	= Poisson's ratio of composite material
σ_a	= allowable axial stress in each lamina

Introduction

ADVANCED composite-stiffened panels are being used more and more extensively in aerospace structures, and a multitude of configurations can be found in practical use.

Received Feb. 20, 1985; presented as Paper 85-0674 at the AIAA/ASME/ASCE/AHS 26th Structures, Structural Dynamics and Materials Conference, Orlando, FL, April 15-17, 1985; revision received Jan. 6, 1986.

*Associate Professor, Department of Aerospace Engineering.

The design of minimum-mass compression panels with different cross sections has been investigated by many researchers to increase the structural efficiency of these panels; as a result, several optimization programs have been developed.[1-7]

Since the PASCO computer program, including VIPASA, was not available outside the United States, the OPIC optimizer computer program was designed to determine the minimum-mass configuration of hat- and blade-stiffened composite panels.[8,9] Although engineering formulas should be used with caution, a simplified theoretical analysis was used to design these panels[3,10,11]; in particular, interaction between stiffener twisting and local buckling modes can occur for blade-stiffened panels. Indeed a rapid solution of the program was possible using this method. A more accurate analysis[12,13] is being studied, and the development of a computer program for the instability of plate assemblies is almost complete.

Regarding experimental tests, several factors affect the comparison between analytical and experimental results, i.e., variations in thickness and material properties, boundary conditions, and geometric imperfections. Furthermore, apparent moduli of laminated composite materials are not necessarily constant with stress[14]; in this case, a tangent modulus theory or equivalent should be used.

Indeed, simple compression tests cannot represent the load condition of a wing-box compression panel properly because of the constraints and deformations induced at the edges included in the structure[15,16]; furthermore, the bending curvature associated with longitudinal load causes a distributed load perpendicular to panels that can reduce longitudinal load at which buckling occurs.

Design and Analysis of Stiffened Compression Panels

Hat- and blade-stiffened panels under uniaxial compression were considered in the present investigation; cross-sectional configurations are shown in Fig. 1. Unidirectional and 45 deg plies are placed so as to have a balanced and symmetric laminate. The preceding stacking sequence was selected as it was shown[2,3] to give better structural efficiency. The geometric variables of a cross section are width and thickness of each layer of each element.

Buckling Analysis

Euler, local and twisting loads, and strain at which the panels buckle, were determined independently from each other, not taking into account interactions between these three modes. For the closed stiffened section, the twisting buckling mode was not considered; for blade-stiffened sections, in

which the axis of rotation is located at the intersection of the skin symmetrical axis with the stiffener symmetrical axis, there is no interaction between torsion and flexure.[17,10]

Overall Buckling

The longitudinal overall buckling load per unit width was evaluated by solving the general differential equation for the deflection surface of an orthotropic plate with all edges simply supported:

$$Nx_{cr} = (\Pi^2/\lambda^2)[D_1 + 2D_3(\lambda/\mu)^2 + D_2(\lambda/\mu)^4]$$

the smeared orthotropic stiffnesses involved are the bending stiffnesses D_1 and D_2 and the twisting stiffness D_3[3].

The wide-column theory was applied in the experimental tests since panels were simply supported at the compression-loaded edges and free at the sides. The critical load was evaluated with only one pitch of the stiffener spacing and included the effect of the shearing force on the deflection of the column[3,17]:

$$Nx_E = (\Pi^2 EI/pL^2)(1 + \Pi^2 EI/L^2 b_i A_{66_i})$$

Only the stiffener webs were considered to contribute to the shearing effect. The bending stiffness EI was evaluated with respect to an axis parallel to reference one (see Fig. 1) and through the centroid of the section.

Local Buckling

The orthotropic buckling equations for elements with all edges simply supported and for elements having one edge free are, respectively, given by[11]:

$$\begin{aligned} Nx_{li} &= (2\Pi^2/b_i^2)(\sqrt{D_{11}D_{22}} + D_{12} + 2D_{66})_i \\ Nx_{li} &= 12D_{66_i}/b_i^2 + \Pi^2 D_{11_i}/L^2 \end{aligned} \qquad (1)$$

The accuracy of these equations has been investigated by Spier[11] by correlation to experimental data with the conclusion that for some values of b/t the experimental buckling load may be several times larger than predicted. Indeed, for low values of b/t the experimental buckling load may be lower than predicted and the transverse shear effect should have to be included.

Torsional Buckling

The equation of equilibrium of moments about the axis of rotation for the twisted strut subjected to end load and the restraint of the torque spring K_R were studied in Ref. 10. As for blade-stiffened panels the warping stiffness is zero, the strain at which torsional buckling occurs is in the form

$$\epsilon_{tors} = [GJ + K_R(\lambda/\Pi)^2]/EI_0$$

The torsional stiffness was calculated by the expression $GJ = 4\Sigma_i(D_{66}b)_i$ in which the summation is relative to both the skin and stiffener considering that the skin was unbuckled.

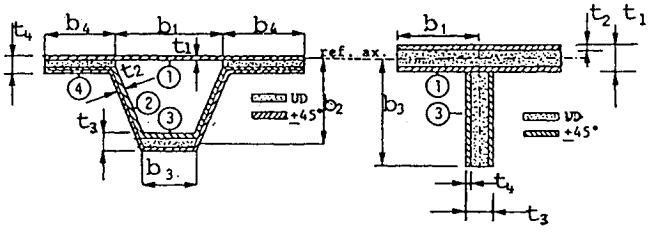

Fig. 1 Configurations and design variables.

Design and Optimization Program

A simplified computer program was designed for the minimum-mass optimization of hat- and blade-stiffened panels; the computer code, denoted OPIC, used an operational procedure in which the geometric variables (widths and thicknesses of each layer of each cross-sectional element) were automatically increased between lower and upper limits by choosing certain steps. For each prescribed axial-load index the overall, local, and torsional buckling were not to be exceeded, although the composite structure has, in some cases, a postbuckling strength. Furthermore, a maximum allowable axial strain for graphite/epoxy material and a maximum allowable axial stress for aramid/epoxy material were not to be exceeded, as well as the material failure stress and strain in each lamina of each plate element. In Fig. 2, the structural efficiency obtained by the OPIC code is reported for panels 762 mm long. Material properties used in the analysis were: Gr/E:$E_{11} = 138$ GPa, $E_{22} = 14.2$ GPa, $G_{12} = 5.24$ GPa, $\nu_{12} = 0.314$, $\epsilon_a = 0.006$ m/m; Ar/E:$E_{11} = 72.4$ GPa, $E_{22} = 5.4$ GPa, $G_{12} = 2.1$ GPa, $\nu_{12} = 0.34$, $\sigma_a = 274$ MPa.

The results obtained for graphite/epoxy hat-stiffened panels were almost the same as the PASCO results[18]; in comparison with the wide column theory a load 15% higher was possible for six stiffener wide panels; for ten stiffener wide panels the difference decreased, at the lowest index, at 7%.

The results obtained for blade stiffened panels were almost 10% heavier than the PASCO results. The PASCO program used a more rigorous buckling analysis (than the simplified buckling equations reported herein) obtaining, for open-section stiffened panels, a better structural efficiency. Structural efficiency results of aramid/epoxy hat-stiffened panels were comparable to that of graphite/epoxy blade-stiffened panels.

Experimental Results and Analytical Comparison of Uniaxial Compression Tests

Four hat-stiffened panels and seven blade-stiffened panels were tested in uniaxial compression to verify the correlation between the preceding theoretical analysis and experimental results. Specimens were designed independently from the optimization results, and their structural efficiency cannot be compared with the results of Fig. 2.

Specimens were manufactured by using graphite/epoxy prepregs in either tape or fabric form. All specimens were vacuum bagged and autoclave cured. Panels and cross-sectional real dimensions are listed in Table 1. Designs H-1 through H-4 are for hat-stiffened panels (specimen H-1 cap had the 0 deg plies outside the ±45 deg plies); designs B-1 through B-7 are blade-stiffened panels. Plain weave fabrics were used for manufacturing the specimens, except for designs H-3, H-4, and B-5 through B-7, which used an eight-harness satin fabric.

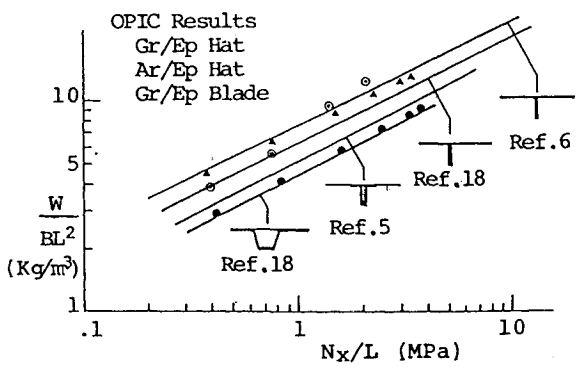

Fig. 2 Structural efficiency of stiffened panels under uniaxial compression.

Panels H-3, H-4, and B-5 through B-7 were slightly curved. The ends of the specimens were potted in a 2-cm-thick block of epoxy resin to obtain parallel and flat ends. It was evident from the test results that it was not always possible to obtain uniform load distributions over the cross section. Unloaded edges were free; skin free edges were cut back, except for designs H-3 and H-4, to prevent their local buckling.

Several strain gages were bonded to the panel elements to measure in-plane strain. Out-of-plane displacements were monitored by the shadow moiré method, and fringe patterns were recorded by a camera. The critical load and strain at which a panel displayed torsional, local, or Euler buckling were defined by load-strain curves together with moiré fringe patterns (when developed), and panel deformations.

Analytical results were based on the following material properties for tape: $E_{11}=131$ GPa, $E_{22}=13$ GPa, $G_{12}=6.4$ GPa, $\nu_{12}=0.38$; and fabric: $E_{11}=E_{22}=63.7$ GPa, $G_{12}=6.4$ GPa, $\nu_{12}=0.08$.

A summary of the results for hat- and blade-stiffened panels is reported in Table 2. Analytically determined strains cor-

Table 1 Panel and cross-section dimensions, cm

Design	Length	Width	b_1	b_2	b_3	b_4	t_1	t_2	t_3	t_4	b_1/t_1	b_2/t_2	b_3/t_3	b_4/t_4
H-1	75.0	25.6	3.00	3.10	1.80	2.85	0.065	0.065	0.425	0.255	46.2	47.7	4.2	11.2
H-2	84.0	30.5	2.80	3.00	1.85	2.50	0.080	0.080	0.600	0.300	35.0	37.5	3.1	8.4
H-3	29.2	39.5	2.92	2.99	2.24	2.33	0.136	0.136	0.313	0.353	21.5	22.0	7.2	6.6
H-4	51.1	39.5	2.92	2.99	2.24	2.33	0.136	0.136	0.313	0.353	21.5	22.0	7.2	6.6
B-1	15.0	30.5	4.23		3.15		0.195	0.076	0.361	0.038	21.7		8.7	
B-2	25.0	30.5	4.23		3.15		0.195	0.076	0.361	0.038	21.7		8.7	
B-3	36.5	30.5	4.23		3.15		0.195	0.076	0.361	0.038	21.7		8.7	
B-4	65.0	30.4	4.25		3.05		0.206	0.084	0.346	0.042	20.7		8.8	
B-5	33.5	48.7	4.23		3.05		0.343	0.151	0.376	0.086	12.4		8.1	
B-6	45.2	48.9	4.24		3.03		0.327	0.143	0.370	0.083	13.0		8.2	
B-7	66.5	48.7	4.22		3.19		0.300	0.130	0.300	0.050	14.1		10.6	

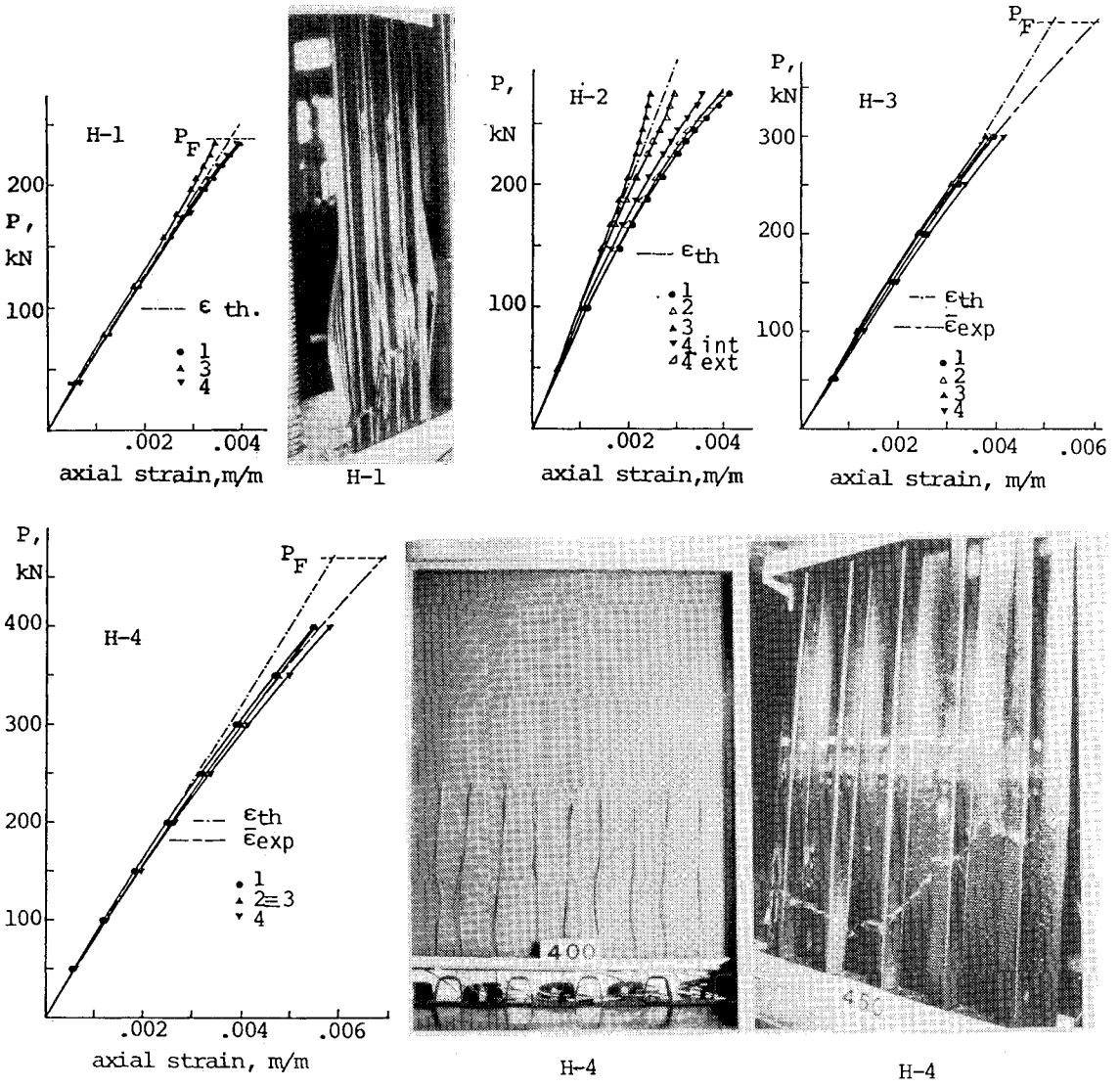

Fig. 3 Experimental results of hat-stiffened panels under uniaxial compression.

Table 2 Buckling results for hat- and blade-stiffened panels

Panel design	Analytical results: Buckling strain, m/m	Analytical results: Buckling mode	Experimental results: Avg. buckling strain, m/m	Experimental results: Avg. failure strain[a], m/m	Experimental results: Failure load, kN
H-1	0.00354	Euler	0.00360	0.0039	238.4
H-2	0.00264	Euler	0.00286	0.0038	314.0
H-3	0.00860	Local (free element 4)	—[c]	0.0061	417.0
H-4	0.00698	Euler	—[c]	0.0069	470.0
B-1	0.00203	Torsional	0.00189	0.0026	196.2[b]
B-2	0.00196	Torsional	0.00173	0.0028	196.2
B-3	0.00218	Torsional	0.00221	0.0025	196.2[b]
B-4	0.00220	Euler	0.00225	0.0038	236.4
B-5	0.00548	Local (element 3)	0.00475	0.0060	530.7
B-6	0.00432	Euler	0.00442	0.0050	443.4
B-7	0.00220	Euler	0.00216	0.0022	211.4

[a]Values extrapolated from load-strain curves. [b]No failure occurred at the maximum test load. [c]No strain reversal occurred up to the measured strain.

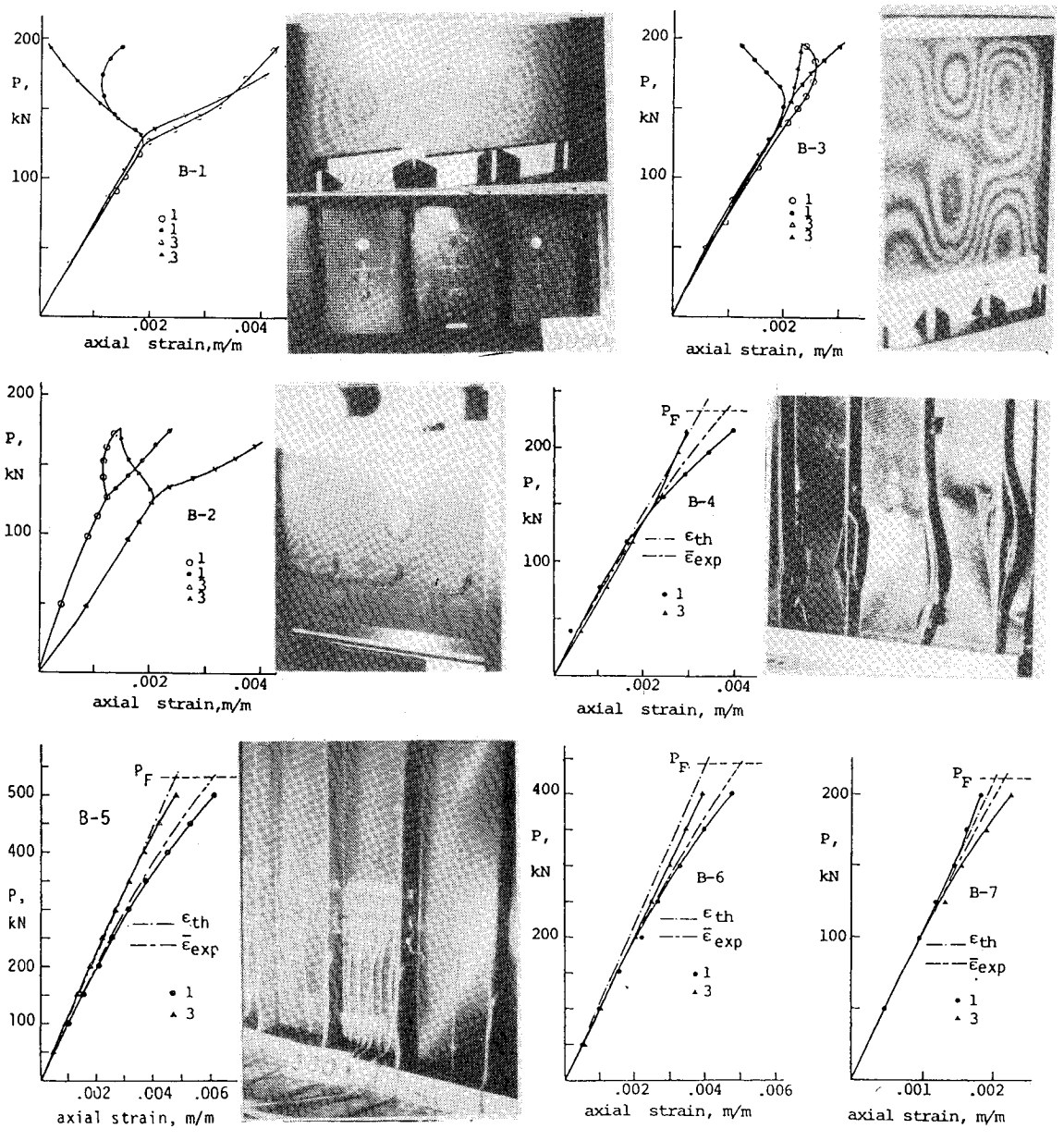

Fig. 4 Experimental results of blade-stiffened panels under uniaxial compression.

responding to Euler, local, or torsional buckling modes are reported. The smeared extensional stiffness was used to calculate the corresponding critical load or, vice versa, to calculate axial strain; for compatibility, the strain in each panel element was assumed to be equal. Average strain values from several strain gages are reported for each test. Load-strain curves, except for some tests, are extrapolated up to the failure load to obtain the average failure strain. The linearly elastic load-strain curve is also shown.

Hat-Stiffened Panels

Design H-1 is a three-stiffener-wide panel, design H-2 a four-stiffener-wide panel, and designs H-3 and H-4 five-stiffener-wide panels. The shadow moiré method was not used for specimens H-1 and H-2. Experimental load-strain curves and pictures are given in Fig. 3.

Design H-1

An almost linear behavior was recorded nearly up to the failure load; a reversal strain began at an axial load of 226 kN and at an average strain of 0.0036. The specimen failed in an explosive fashion and a large amount of unidirectional fiber splinters were expelled.

Design H-2

A strain reversal is very clear at an axial load of 260 kN and at average experimental strains of 0.00286. The specimen carried load beyond the onset of overall buckling and failure occurred near one end.

Design H-3

Failure occurred at an axial load far lower than the analytical one; indeed, beginning at a load of 200 kN, moiré patterns were developed in element 1 of the central stiffener; a strain gage placed on this element recorded a linear behavior up to a load of 300 kN, thereafter measurements were stopped. The failure occurred by delamination of the skin at a load lower than predicted; indeed, since the low value $b/t = 6.6$ of free edges (element 4), the transverse shear effect had an important role in the failure of the specimen.

Design H-4

The specimen failed at an extrapolated average axial strain of 0.0069, corresponding to the analytically determined overall buckling strain. Beginning at a load of 300 kN, moiré patterns were noted in element 1 of three stiffeners. At high loads a strain divergence was measured by strain gages placed in the center of the panel. A nonlinear behavior seems very clear, especially at higher strains.

Blade-Stiffened Panels

Designs B-1 through B-4 were four stiffener wide panels; designs B-5 through B-7 were six stiffener wide panels. Experimental load-strain curves and pictures are given in Fig. 4.

Design B-1

A strain reversal is very clear at an axial load of 137.3 kN at which the moiré pattern was slightly developed and antisymmetrical stiffener twisting noted. Clamped boundary conditions were produced by the ends. The specimen carried the load beyond the onset of buckling, and a well-developed pattern was monitored. No failure occurred at the maximum test load.

Design B-2

The same behavior as panel B-1 was noted. Lower strains in the skin with respect to those in the stiffeners were recorded at a 137.3 kN axial load. Two half-wave patterns were well developed at 186.4 kN, and the specimen failed in an explosive fashion at an axial load of 196.2 kN.

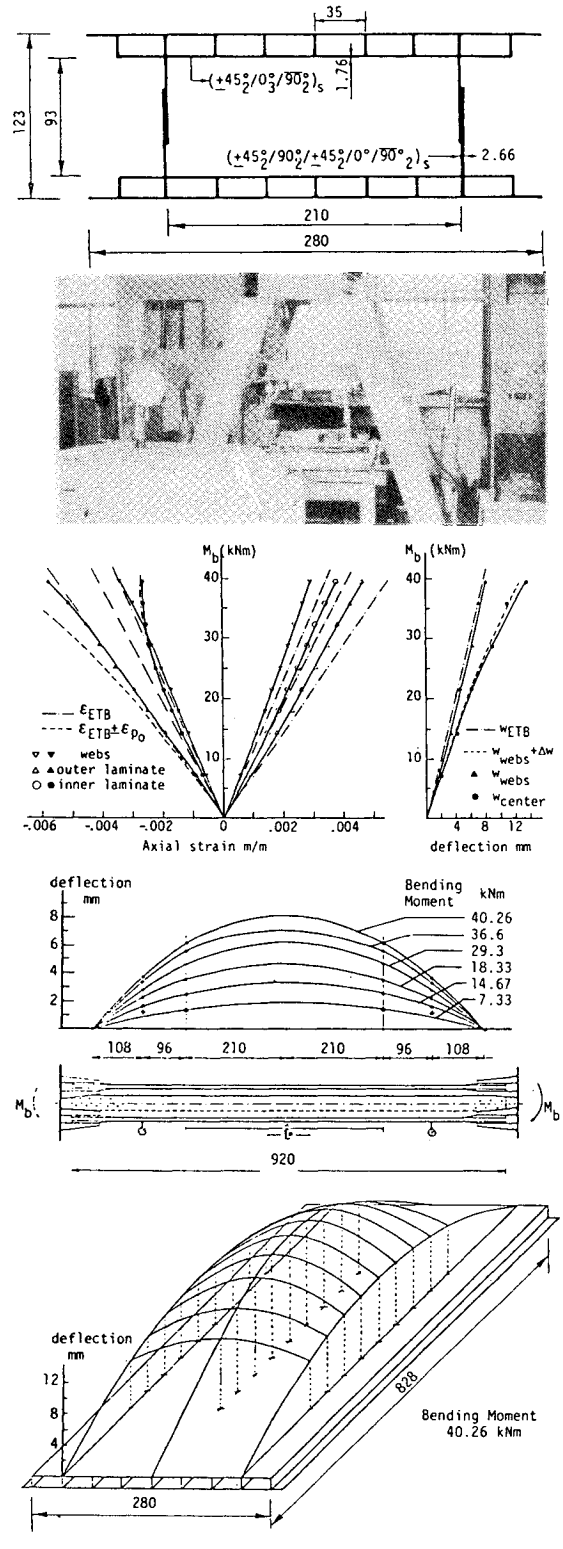

Fig. 5 Experimental results of cellular panels wing box under pure bending.

Design B-3

A two half-wave antisymmetrical torsional mode was very clear at a load of 166.8 kN and an average strain of 0.00221. The specimen carried load beyond the onset of buckling; no failure occurred at maximum test load.

Design B-4

A divergence of skin and stiffener average strain is evident at an axial load of around 150 kN and a strain of 0.00225, cor-

responding to the analytically predicted Euler strain. Panel out-of-plane deflections were also indicated by moiré fringe patterns. Additional fringes were slightly developed near the lower end at an axial load of 216 kN, and an explosive failure in this region occurred at a load of 236.4 kN.

Design B-5

Moiré patterns were developed at an axial load of 450 kN, and blade local buckling was noted at 500 kN based on observed strain reversals. Stiffener local buckling occurred at a strain lower than predicted as a consequence of the low value of $b/t = 8.1$. The specimen failed in an explosive fashion at an axial load of 530.7 kN when the skin disbonded from the stiffeners.

Design B-6

Panel deflection was indicated by moiré patterns at an axial load of 400 kN and an average strain of 0.00442, corresponding with the analytical Euler strain; the structure had a postbuckling strength and failure occurred when stiffener local buckling interacted with overall buckling.

Design B-7

The analytically determined stiffener buckling strain (0.00230) was very close to the overall buckling strain; the specimen did not have any postbuckling strength and failed immediately by local buckling.

Wing Box in Bending

Some experimental and analytical results are available in the literature on composite-stiffened panels under combined loads, different constraints at edges, and effects of bow-type initial imperfection. However, the panels themselves are considered isolated from the main structure; indeed, boundary conditions at the edges are not always well known and, furthermore, deformations could be included at the edges from the other substructures.

Deformations of wing-box compression panels were analytically investigated[15,19] using a differential equation of an orthotropic plate with lateral pressure, initial imperfection, and flexural deformation of bulkheads introduced into the analysis by a Fourier series. Experimental results[16] on several aluminum-alloy wing-box beams in bending showed remarkable deformations of panels (particularly the compressed ones) in a direction normal to their barycentric surface affecting both local stresses and final failure load.

Additional loads are created on a wing-box compression panel when bending loads are applied on the beam; bending curvature, associated with longitudinal load, causes a distributed load perpendicular to both upper and lower wing-box panels resulting in a compressive loading. The bending curvature will not be constant along the transverse direction but will reach a maximum value in the center of the two webs. This perpendicular load can play an important role on strain distribution, reducing the longitudinal load at which buckling could occur.

Experimental Results and Analytical Comparison of Bending Tests

Starting from the preceding considerations, pure bending tests were carried out on wing-box beams. Two specimens had cellular cross-sectional panels; a 4-m-long similar structure manufactured several years ago by aluminum-alloy material[20] showed the feasibility of an integral ribless wing. The lamina stacking sequence and dimensions of the second wing box are sketched in Fig. 5. Each panel was manufactured combining thermal expansion rubber cores with an autoclave-controlled pressure cycle. Graphite/epoxy prepreg material was used. The wing boxes were 92.0 cm long; a 50% mass saving was obtained in comparison with the similar aluminum wing box. Each panel was reinforced at the ends by glass/epoxy for a length of 14 cm.

A third specimen had an unstiffened orthotropic panel; the lamina stacking sequence and dimensions are sketched in Fig. 6; graphite/epoxy prepreg material was used and cured by an autoclave-controlled pressure cycle; the wing box was 82 cm long.

Suitable fittings were bolted at the ends in order to attach them to the bending machine. Specimens were bolted by two clamps hinged to the frame by four rods; on the other side of each clamp a hydraulic jack was hinged so that the bending moment could be applied. Deflection data at different load levels were taken using a dial deflectometer which ran on a guide for a length of approximately 42.5 cm and was connected to an x-y recorder; additional dial deflectometers were placed near the ends. Longitudinal strains were measured by several strain gages placed at half-length. The applied bending moment was increased step by step to record the deflection curves and the strain measurements at constant loads.

Cellular Panel Wing Box

Results of the second specimen are reported in Fig. 6; deflection curves at different values of the bending moment showed a maximum deflection at the sides varying linearly with load. Experimental deflections were slightly lower than the analytical ones calculated by the Engineer's Theory of Bending (ETB). Higher curvatures were drawn in the longitudinal middle section as an effect of distributed perpendicular load; deflections of a simply supported orthotropic plate under distributed lateral load were calculated in the following form[21]:

$$W = \frac{16p_0}{\Pi^4}\left\{\left[\sum_{m=1,3,5}^{\infty}\sum_{n=1,3,5}^{\infty}\frac{1}{mn}\sin\frac{m\Pi x}{a}\sin\frac{n\Pi y}{b}\right]\Big/\left[D_{11}\left(\frac{m}{a}\right)^4 + 2\left(D_{12}+2D_{66}\right)\left(\frac{m}{a}\right)^2\left(\frac{n}{b}\right)^2 + D_{22}\left(\frac{n}{b}\right)^4\right]\right\}$$

(terms up through $m = 5$ and $n = 5$ were used).

Additional middle maximum deflections resulted that were closely related to the experimental ones, except for the value before failure.

Compared to ETB, longitudinal strains vs bending moment curves show an ever-growing strain reduction in the inner laminate of the compression panel; the analytical results were in close agreement with the experimental results for the inner laminate, taking into account the effect of lateral pressure on the strain distribution of stiffened compression panels[22]; however, analytical results were rather different from the experimental ones for the outer laminate, and the difference increased at the higher loads. Shifting of the neutral axes toward the tensile panel was measured. Based on Eq. (1), local buckling of the laminate of each cell could have occurred at an axial strain of 0.0070. Failure occurred at a bending moment of 42 kNm, corresponding to an axial strain of around 0.00650 (extrapolated from the curves). The 16% lower load could be associated with a few defects in the corners (resin pockets), giving rise to the delamination of the outer laminae of the laminates. Furthermore, a more complex stress distribution could arise at the interface between the laminates and the sides of each cell as an effect of the compressive loading, including normal and transverse shear stresses.

Similar behavior was recorded for the first specimen, which failed at a load of 33 kNm; indeed, it was slightly thinner and, in particular, had 0/90 deg fabric plies instad of 90 deg tape plies in the skin, reducing transverse bending stiffness.

Unstiffened Panel Wing Box

Experimental results are reported in Fig. 6. Measured surface strain data from back-to-back strain gages and computed membrane strain are plotted for several bending-moment values. Strain gages were placed on both panels and in the webs in the middle length only. A bow-type initial imperfec-

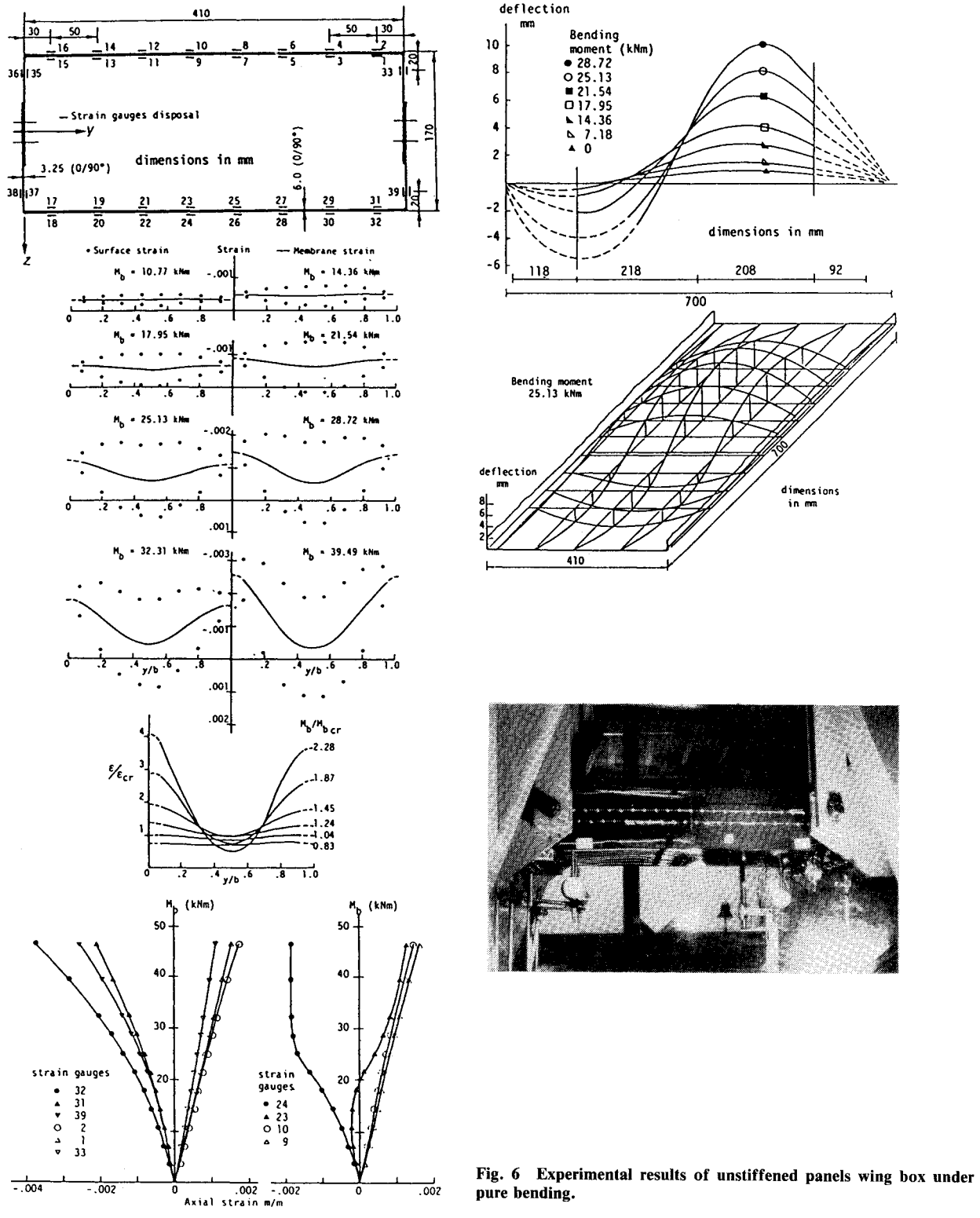

Fig. 6 Experimental results of unstiffened panels wing box under pure bending.

tion was recorded in the compression panels, and the highest values measured were 1 mm at the middle width and 0.1 mm at the edge.

A maximum membrane strain of 0.00062 was achieved in the middle longitudinal section at a bending moment of 21.54 kNm, after which they began to reduce. High strains were recorded at the edges as the applied load increased. Based on the orthotropic buckling equations for a simply supported plate, buckling should have occurred in two half-waves at a longitudinal strain of 0.00049; however, because the plate aspect ratio was 1.61, the nearest buckling form was one half-wave at a longitudinal strain of 0.00063. From the bending moment vs strain curves, a reversal is very clear in strain-gage 23 at a bending moment of 14.36 kNm, which corresponds to a membrane strain of 0.00046. This value was in good agreement with the analytically predicted buckling strain of the plate; however, increasing the bending moment up to a value of 21.54 kNm produced the maximum membrane strain of 0.00062 and the panel was one half wavelength higher than the one corresponding to a two half-wave symmetrical buckle mode. The difference between the loads at which the strain reversal and the maximum membrane strain occurred can be

attributed to the distributed perpendicular load. In fact, it is very clear because, in the middle section of the tensile panel, the inner-surface strain (gage 9) had a higher value than the outer one (gage 10), while at the edges the perpendicular load did not affect the strain distribution. The experimental buckling load was higher than the analytical one since the edge stiffening was probably different from the simply supported hypothesis; however, it seems that the initial imperfection made the buckling corresponding to a higher strain energy possible (barrel effect). Deflection curves taken near the webs showed a linear relation with the load, and in close relationship with the ETB, up to a bending moment of 21.54 kNm, beyond which the usual bending curvature was no longer kept.

Conclusion

Adequate correlation between analytical and experimental results were obtained for uniaxial compression tests when Euler or torsional buckling modes were critical. The experimental average strains corresponding to the buckling load were considered instead of theoretical linear strains; in fact, as a consequence of the non-Hookean behavior of some composite materials, extensional and bending stiffnesses of laminates decreased as the load increased. In some cases, the structures tested showed a remarkable postbuckled strength. Indeed, when the local buckling mode was critical, failure occurred at a load lower than the analytical predicted buckling load as an effect of the transverse shear stress for low values of b/t. The buckling formulas reported herein should be used with caution; in fact, an interaction between the three modes is possible when the buckling loads of each mode are very close to each other. A more accurate analysis is being studied to take this effect into account.

Wing-box beams tested in pure bending showed that, as strain distribution and curvatures are affected by the distributed load perpendicular to the panels caused from the bending curvature, an adequate correlation with the analytical results was obtained taking into account the orthogonal pressure. The experimental beam deflections were in close agreement with the analytical ones calculated by the Engineer's Theory of Bending.

Acknowledgments

The author would like to acknowledge the efficacious cooperation of G. Celotto, C. Brovarone, L. Zannetti, E. Bonadero, S. Fassio, and M. Bettinardi (last year's undergraduates in aeronautical engineering), and G. Ruvinetti and E. Fiscelli (technical staff). Thanks also to the staff of the C. Grassi Technical High School for the autoclave support, and to Professor E. Antona for his helpful advice.

References

[1]Williams, J. G. and Mikulas, M. M., "Analytical and Experimental Study of Structurally Efficient Composite Hat-Stiffened Panels Loaded in Axial Compression," AIAA Paper 75-754, May 1975.

[2]Agarwall, B. and Davis, R. C., "Minimum Weight Designs for Hat Stiffened Composite Panels Under Uniaxial Compression," NASA TN D-7779, 1974.

[3]Stroud, W. J. and Agranoff, N., "Minimum Mass Design of Filamentary Composite Panels Under Combined Loads: Design Procedure Based on Simplified Buckling Equations," NASA TN D-8257, 1976.

[4]Stroud, W. J. and Agranoff, N., "Minimum Mass Design of Filamentary Composite Panels Under Combined Loads: Design Procedure Based on a Rigorous Buckling Analysis," NASA TN D-8417, 1977.

[5]Stein, M. and Williams, J.G., "Buckling and Structural Efficiency of Sandwich Blade Stiffened Composite Compression Panels," NASA TP 1269, 1978.

[6]Williams, J. G. and Stein, M., "Buckling Behavior and Structural Efficiency of Open Section Stiffened Composite Compression Panels," *AIAA Journal*, Vol. 14, Nov. 1976, pp. 1618-1623.

[7]Anderson, M. S. and Stroud, W. J., "A General Sizing Computer Code and Its Application to Composite Structural Panels," AIAA Paper 78-467, 1978.

[8]Romeo, G., "Design of Hat Stiffened Composite Panels Under Uniaxial Compression and Shear Minimum-Mass Optimization Based on a Simplified Theory," Department of Aerospace Engineering, Delft University of Technology, Delft, the Netherlands, Rept. LR 312, Jan. 1981.

[9]Romeo, G., "Risultati Teorici Sperimentali di Pannelli Integrali in Materiale Composito Soggetti a Compressione e Taglio" ("Theoretical and Experimental Results of Composite Stiffened Panels Under Uniaxial Compression and Shear"), AIDAA, VIIth National Congress, Naples, Oct. 1983.

[10]Argyris, J. H., "Flexure-Torsion Failure of Panels," *Aircraft Engineering*, Vol. 27, June 1954, pp. 174-184.

[11]Spier, E. E., "On Experimental versus Theoretical Incipient Buckling of Narrow Graphite/Epoxy Plate in Compression," AIAA Paper 80-686, 1980.

[12]Wittrick, W. H. and Williams, F. W., "Buckling and Vibration of Anisotropic or Isotropic Plate Assemblies Under Combined Loadings," *International Journal of Mechanical Science*, Vol. 16, April 1974, pp. 209-239.

[13]Wittrick, W. H., "General Sinusoidal Stiffness Matrices for Buckling and Vibration Analyses of Thin Flat Walled Structures," *International Journal of Mechanical Science,* Vol. 10, 1968, pp. 949-966.

[14]Van Dreumel, W. H. M. and Kamp, J. L. M., "Non-Hookean Behaviour in the Fibre Direction of Carbon Fibre Composites and the Influence of Fibre Waviness on the Tensile Properties," *Journal of Composite Materials*, Vol. 11, Oct. 1977, p. 461.

[15]Antona, E. and Pelagalli, P., "Analisi Strutturale dei Cassoni Alari Bilongheroni Soggetti a Flessione in Campo Elastico" ("Structural Analysis of Two Spars Wing Boxes Having an Elastic Behavior Under Bending"), Politecnico di Torino, Istituto di Progetto di Aeromobili, Rept. 49, Dec. 1968.

[16]Antona, E. and Gabrielli, G., "An Experimental Investigation on Wing Box Beams in Bending," ICAS Paper 70-83, Sept. 1970.

[17]Timoshenko, S. P. and Gere, J. M., *Theory of Elastic Stability*, McGraw-Hill Book Co., New York, 1961.

[18]Williams, J. C., Anderson, M. S., Rhodes, M. D., Starnes, J. H. Jr., and Stroud, W. J., "Recent Development of the Design, Testing and Impact Damage Tolerance of Stiffened Composite Panels," NASA TM 80077, April 1979.

[19]Antona, E., "Effetto della Pressione Ortogonale e Fenomeni d'Instabilitá Globale nei Pannelli Compressi dei Cassoni Alari Centinati Soggetti a Flessione" ("Effect of Orthogonal Pressure and Overall Buckling Phenomena on Wing Boxes Compression Panels under Bending"), Politecnio di Torino, Istituto di Progetto di Aeromobili, Rept. 40, Oct. 1967.

[20]Morelli, P. and Romeo, G., "Experimental Investigation into the Feasibility of an Extruded Wing," *Proceedings of the Symposium on Science and Technology of Low Speed and Motorless Flight*, NASA CP 2085, Pt. II, March 1979, pp. 419-436.

[21]Jones, R. M., *Mechanics of Composite Materials*, McGraw-Hill Book Co., New York, 1975.

[22]Giles, G. L. and Anderson, M. S., "Effects of Eccentricities and Lateral Pressure on the Design of Stiffened Compression Panels," NASA TND 6784, June 1972.